ACS OMEGA

http://pubs.acs.org/journal/acsodf

Article

High-Pressure-Limit Rate Coefficients for HO_2 Elimination Reactions of Hydroperoxyalkenylperoxy Radicals based on the Reaction Class Transition State Theory

XiaoHui Sun,* ZhenYu Pei, and ZeRong Li

Cite This: *ACS Omega* 2022, 7, 20020−20031

Read Online

ACCESS | Metrics & More | Article Recommendations | Supporting Information

ABSTRACT: Thermokinetic parameters and transport parameters are of great importance to the combustion model and the reaction rate rules are of great importance to construct the combustion reaction mechanism for hydrocarbon fuels. The HO_2 elimination reaction class for hydroperoxyalkenylperoxy radicals is one of the key reaction classes for olefin, for which the rate coefficients are lacking. Therefore, the rate coefficients and rate rules of the HO_2 elimination reaction class for hydroperoxyalkenylperoxy radicals are studied in this work. The reaction class transition state theory (RC-TST) is used to calculate the rate coefficients. In addition, the HO_2 elimination reaction class of hydroperoxyalkenylperoxy radicals is divided into four subclasses depending upon the type of H−C_β bond that is broken in the reactant molecules, and the rate rules are calculated by taking the average of rate coefficients from a representative set of reactions in a subclass. The calculated kinetics data would be valuable for the construction of the combustion reaction mechanism for olefin.

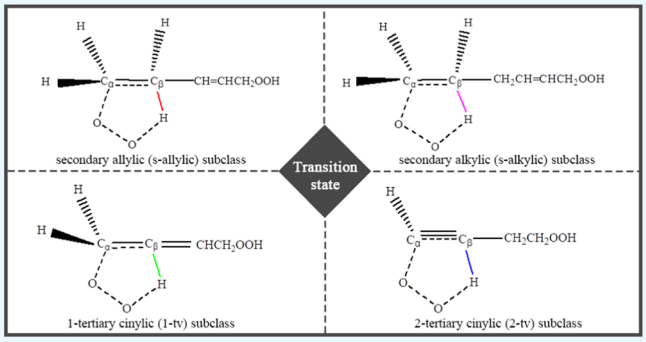

1. INTRODUCTION

A detailed understanding of the combustion model of hydrocarbon fuels plays a key role in exploring the reduction of the emissions from pollutants during combustion and may lead to cleaner and more efficient strategies in automotive vehicle and fuel design.[1] Meanwhile, the detailed kinetic model of combustion or pyrolysis for hydrocarbon fuels is of great significance to study the ignition phenomena, reactive flows, and so on.[2−8] However, there has been little kinetic modeling for unsaturated hydrocarbon fuels[4,9,10] compared to the extensive studies for saturated hydrocarbon fuels. It is valuable to study the impact of the C=C double bond on the reaction mechanism of unsaturated hydrocarbon fuels through theoretical and experimental studies.[3,11−14] In general, a complete reaction mechanism is composed of two parts: one is the core mechanism, which involves reactions of small molecules with no more than 4 carbon atoms and are common for all hydrocarbons. The other part is the expanded mechanism, which involves reactions of large molecules; these reactions are always divided into different reaction classes according to the similarities of the potential energy surfaces along their reaction coordinates[15,16] and are constructed in a systematic way by software on the basis of the rate estimation rules.[3,17−27] In the generation of the reaction mechanism, a complete and reasonable reaction list, accurate thermokinetic parameters, and transport parameters are essential.[3,16,28] It is widely accepted that the reaction mechanism in the low-temperature region is complex due to the large number of species and elementary reactions.[1,3,29−34]

Olefins are one of the important components of transportation fuels and important intermediates during the combustion process for alkanes.[11,35] Analogous to the low-temperature oxidation process for alkanes, olefins first undergo hydrogen extraction reaction to form alkenyl radicals ($R^\bullet$), followed by oxidation to produce alkenylperoxy radicals ($ROO^\bullet$). The hydroperoxyalkenyl radicals ($^\bullet QOOH$) are produced through the intramolecular H-shift of alkenylperoxy radicals ($ROO^\bullet$). Then, the $^\bullet QOOH$ radicals add to a second oxygen molecule to produce $^\bullet O_2QOOH$ (hydroperoxyalkenylperoxy) radicals.[36,37] The main reaction paths for olefin are schemed in Figure 1, where R, $R^\bullet$, and Q represent the olefin molecules (C_nH_{2n}), alkenyl radicals (C_nH_{2n-1}), and a chain with 2 H-atoms replaced by olefin molecules (C_nH_{2n-2}), respectively. Nowadays, experimental measurements and mechanism studies for ethylene,[38−43] propene,[44−47] butene,[48−50] and other large olefins[51−53] are being undertaken, including low- and high-temperature kinetic schemes. Up to now, there have been some

Received: March 24, 2022
Accepted: May 19, 2022
Published: June 3, 2022

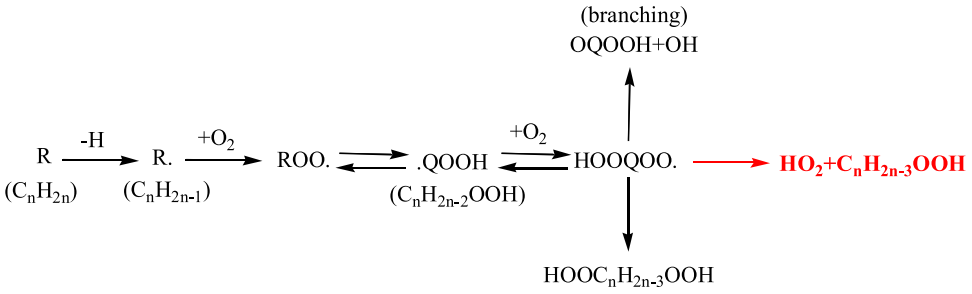

Figure 1. Reaction pathways of olefin.

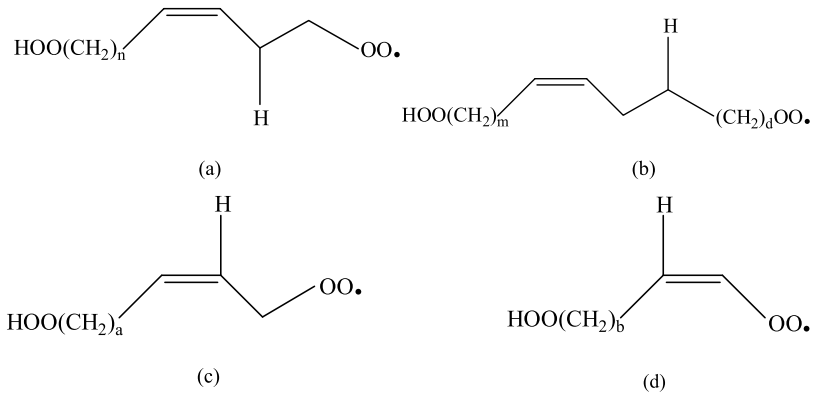

Figure 2. Types of C−H bonds in a reactant molecule: (a) secondary allylic C−H bond; (b) secondary alkylic C−H bond; (c) 1-tertiary vinylic C−H bond; and (d) 2-tertiary vinylic C−H bond.

theoretical studies of alkanes and their radicals by RC-TST,[54] wherein the thermokinetic parameters for large molecular systems are obtained by a low-level *ab initio* method.

For the HO_2 elimination reaction of hydroperoxyalkenylperoxy radicals, the C_α−OO and H−$C_\beta C_\alpha$OO bonds are broken. Similar to the work[1,16,28] on olefins and their radicals, the H−C_β bonds in this work are divided into allylic C−H bonds (i.e., the C−H bond is attached to the α position of the C=C double bond) and vinylic C−H bonds (i.e., the C−H bond on the C=C double bond). Analogous to the classification method of alkanes and their radicals,[55] a carbon atom that connects with three hydrogen atoms is defined as a primary ("p") section, and a carbon atom that connects with two hydrogen atoms and one hydrogen atom is defined as secondary ("s") and tertiary ("t") sections, respectively. The types of C−H bonds studied in this work include the secondary allylic C−H bonds, secondary alkylic C−H bonds, and tertiary vinylic C−H bonds, which are shown in Figure 2. It is worth noting that the tertiary vinylic C−H bonds are artificially divided into 1-tertiary vinylic C−H bonds and 2-tertiary vinylic C−H bonds to distinguish the different transition states formed from the tertiary vinylic C−H bonds. Among them, the 1-tertiary vinylic C−H bond has a CH_2 group between it and the OO radicals, and the 2-tertiary vinylic C−H bond is directly linked to the vinyl CH group.

It is well known that the reaction mechanisms are usually developed automatically by software based on the reaction rate rules.[56−60] In order to reduce the uncertainty of the rate rules, the reaction class is usually divided into different reaction subclasses according to the reaction characteristics for the subclasses. Then, the rate rules are calculated by taking the average of the rate coefficients from a representative set of reactions for each subclass.

In this work, 38 reactions for the HO_2 elimination reaction class of hydroperoxyalkenylperoxy radicals are chosen; the reaction list is listed in Table 1. It is worth noting that only the number of carbon atoms involved in the reactions ranging from four to six are studied in this work. In addition, these 38 reactions are divided into "secondary allylic", "secondary alkylic", "1-tertiary vinylic", and "2-tertiary vinylic" reaction subclasses. The terms "s-allylic", "s-alkylic", "1-tv", and "2-tv" are used to represent the different reaction subclasses in the below discussion of tables and figures, and their descriptions will not be repeated. The detailed reaction processes for four reaction subclasses are expressed in Figure 3, where "*n*" (n = 0,1,2,3), "*m*" (m = 0,1,2), "a" (a = 0,1,2,3,4), "b" (b = 2,3,4,5), "d" (d = 1,2,3), and "e" (e = 3,4,5) in the reactant molecules refer to the number of methylenes, with R_a, R_b, and R_c representing the hydrogen atoms or substitutes.

2. COMPUTATIONAL DETAILS AND METHODS

2.1. Computational Details. All *ab initio* calculations are done using the Gaussian 09 package.[61] The geometry optimization and frequency calculation are performed at the B3LYP/6-31+G(d,p) level of theory. The Gaussian-4(G4) method is used as the high-level *ab initio* method. In order to validate the reliability of the G4 method, the single-point energies for reactants, products, and transition states for reactions R21 and R22 are calculated by the benchmark CCSD(T)/cc-pVTZ method.[62,63] In addition, a scaling factor of 0.95 is used to scale the wavenumbers obtained from the frequency analysis.[16,27] The intrinsic reaction coordinate (IRC) analysis is used to confirm the reaction process and the corresponding reactants and products of the transition state belonging to the reaction. All of the intrinsic reaction coordinate (IRC) plots are provided in Figure S1 in the supporting information. The illustration of the reaction coordinate changes from IRC for reaction R1 is shown in Figure 4. The low-

https://doi.org/10.1021/acsomega.2c01811
ACS Omega 2022, 7, 20020−20031

Table 1. List of Reactions

reaction subclass	reaction	reaction equation
s-allylic	R1	*cis*-HOOCH=CH(CH_2)$_2$OO$^\bullet$ → HOOCH=CHCH=CH_2 + $HO_2^\bullet$
	R2	*trans*-HOOCH=CH(CH_2)$_2$OO$^\bullet$ → HOOCH=CHCH=CH_2+$HO_2^\bullet$
	R3	*cis*-HOOCH_2CH=CH(CH_2)$_2$OO$^\bullet$ → HOOCH_2CH=CHCH=CH_2 + $HO_2^\bullet$
	R4	*trans*-HOOCH_2CH=CH(CH_2)$_2$OO$^\bullet$ → HOOCH_2CH=CHCH=CH_2 + $HO_2^\bullet$
	R5	*cis*-HOO(CH_2)$_2$CH=CH(CH_2)$_2$OO$^\bullet$ → HOO(CH_2)$_2$CH=CHCH=CH_2 + $HO_2^\bullet$
	R6	*trans*-HOO(CH_2)$_2$CH=CH(CH_2)$_2$OO$^\bullet$ → HOO(CH_2)$_2$CH=CHCH=CH_2 + $HO_2^\bullet$
	R7	*cis*-HOO(CH_2)$_3$CH=CH(CH_2)$_2$OO$^\bullet$ → HOO(CH_2)$_3$CH=CHCH=CH_2 + $HO_2^\bullet$
	R8	*trans*-HOO(CH_2)$_3$CH=CH(CH_2)$_2$OO$^\bullet$ → HOO(CH_2)$_3$CH=CHCH=CH_2 + $HO_2^\bullet$
s-alkylic	R9	*cis*-HOOCH=CH(CH_2)$_3$OO$^\bullet$ → HOOCH=CHCH_2CH=CH_2 + $HO_2^\bullet$
	R10	*trans*-HOOCH=CH(CH_2)$_3$OO$^\bullet$ → HOOCH=CHCH_2CH=CH_2 + $HO_2^\bullet$
	R11	*cis*-HOOCH_2CH=CH(CH_2)$_3$OO$^\bullet$ → HOOCH_2CH=CHCH_2CH=CH_2 + $HO_2^\bullet$
	R12	*trans*-HOOCH_2CH=CH(CH_2)$_3$OO$^\bullet$ → HOOCH_2CH=CHCH_2CH=CH_2 + $HO_2^\bullet$
	R13	*cis*-HOO(CH_2)$_2$CH=CH(CH_2)$_3$OO$^\bullet$ → HOO(CH_2)$_2$CH=CHCH_2CH=CH_2 + $HO_2^\bullet$
	R14	*trans*-HOO(CH_2)$_2$CH=CH(CH_2)$_3$OO$^\bullet$ → HOO(CH_2)$_2$CH=CHCH_2CH=CH_2 + $HO_2^\bullet$
	R15	*cis*-HOOCH=CH(CH_2)$_4$OO$^\bullet$ → HOOCH=CH(CH_2)$_2$CH=CH_2 + $HO_2^\bullet$
	R16	*trans*-HOOCH=CH(CH_2)$_4$OO$^\bullet$ → HOOCH=CH(CH_2)$_2$CH=CH_2 + $HO_2^\bullet$
	R17	*cis*-HOOCH_2CH=CH(CH_2)$_4$OO$^\bullet$ → HOOCH_2CH=CH(CH_2)$_2$CH=CH_2 + $HO_2^\bullet$
	R18	*trans*-HOOCH_2CH=CH(CH_2)$_4$OO$^\bullet$ → HOOCH_2CH=CH(CH_2)$_2$CH=CH_2 + $HO_2^\bullet$
	R19	*cis*-HOOCH=CH(CH_2)$_5$OO$^\bullet$ → HOOCH=CH(CH_2)$_3$CH=CH_2 + $HO_2^\bullet$
	R20	*trans*-HOOCH=CH(CH_2)$_5$OO$^\bullet$ → HOOCH=CH(CH_2)$_3$CH=CH_2 + $HO_2^\bullet$
1-tv	R21	*cis*-HOOCH=CHCH_2OO$^\bullet$ → HOOCH=C=CH_2 + $HO_2^\bullet$
	R22	*trans*-HOOCH=CHCH_2OO$^\bullet$ → HOOCH=C=CH_2 + $HO_2^\bullet$
	R23	*cis*-HOOCH_2CH=CHCH_2OO$^\bullet$ → HOOCH_2CH=C=CH_2 + $HO_2^\bullet$
	R24	*trans*-HOOCH_2CH=CHCH_2OO$^\bullet$ → HOOCH_2CH=C=CH_2 + $HO_2^\bullet$
	R25	*cis*-HOO(CH_2)$_2$CH=CHCH_2OO$^\bullet$ → HOO(CH_2)$_2$CH=C=CH_2 + $HO_2^\bullet$
	R26	*trans*-HOO(CH_2)$_2$CH=CHCH_2OO$^\bullet$ → HOO(CH_2)$_2$CH=C=CH_2 + $HO_2^\bullet$
	R27	*cis*-HOO(CH_2)$_3$CH=CHCH_2OO$^\bullet$ → HOO(CH_2)$_3$CH=C=CH_2 + $HO_2^\bullet$
	R28	*trans*-HOO(CH_2)$_3$CH=CHCH_2OO$^\bullet$ → HOO(CH_2)$_3$CH=C=CH_2 + $HO_2^\bullet$
	R29	*cis*-HOO(CH_2)$_4$CH=CHCH_2OO$^\bullet$ → HOO(CH_2)$_4$CH=C=CH_2 + $HO_2^\bullet$
	R30	*trans*-HOO(CH_2)$_4$CH=CHCH_2OO$^\bullet$ → HOO(CH_2)$_4$CH=C=CH_2 + $HO_2^\bullet$
2-tv	R31	*cis*-HOO(CH_2)$_2$CH=CHOO$^\bullet$ → HOO(CH_2)$_2$C≡CH + $HO_2^\bullet$
	R32	*trans*-HOO(CH_2)$_2$CH=CHOO$^\bullet$ → HOO(CH_2)$_2$C≡CH + $HO_2^\bullet$
	R33	*cis*-HOO(CH_2)$_3$CH=CHOO$^\bullet$ → HOO(CH_2)$_3$C≡CH + $HO_2^\bullet$
	R34	*trans*-HOO(CH_2)$_3$CH=CHOO$^\bullet$ → HOO(CH_2)$_3$C≡CH + $HO_2^\bullet$
	R35	*cis*-HOO(CH_2)$_4$CH=CHOO$^\bullet$ → HOO(CH_2)$_4$C≡CH + $HO_2^\bullet$
	R36	*trans*-HOO(CH_2)$_4$CH=CHOO$^\bullet$ → HOO(CH_2)$_4$C≡CH + $HO_2^\bullet$
	R37	*cis*-HOO(CH_2)$_5$CH=CHOO$^\bullet$ → HOO(CH_2)$_5$C≡CH + $HO_2^\bullet$
	R38	*trans*-HOO(CH_2)$_5$CH=CHOO$^\bullet$ → HOO(CH_2)$_5$C≡CH + $HO_2^\bullet$

frequency vibrations corresponding to the torsions of the single bonds for reactants, transition states, and products are considered in the calculation of the rate coefficients, wherein the one-dimensional (1-D) hindered internal rotors are used to treat the low-frequency vibrations.[62,64,65] The potentials are performed at the B3LYP/6-31+G (d,p) level by a relaxed scan with an interval of 10° for each internal rotation of the reactants and products. For the transition states, the internal rotor scans are only treated with the torsions of single bonds that are not fixed in the transition states. It is worth noting that when the torsion potential is greater than 10 kcal/mol, it is treated as harmonic vibration for the single bonds.[66] The ChemRate software[67] is used to calculate the rate coefficients, and they are fitted to three parameters (A, n, E) over the temperature range of 500 to 2000 K in increments of 100 K according to the modified Arrhenius expression $k = A\cdot T^n\cdot\exp(-E/RT)$, wherein T, R, E, n, and A are the temperature, gas constant, activation energy, temperature coefficient, and pre-exponential factor, respectively. For reactions with high reaction barriers, tunneling correction is often necessary, especially at low temperature. In this work, tunneling correction factors are calculated with an asymmetric Eckart potential.[68−70]

2.2. Computational Methods. The rate coefficients in the transition state theory[71] can be written as $k(T) = \kappa(T)\cdot\sigma\cdot\frac{k_B T}{h}\cdot\frac{Q^{\neq}(T)}{Q^{R(T)}}\cdot\exp\left(-\frac{\Delta V^{\neq}}{RT}\right)$, wherein $\kappa(T)$, σ, k_B, T, h, $Q^{\neq}$, Q^R, $\Delta V^{\neq}$, and R are the tunneling coefficient, reaction symmetry number, Boltzmann constant, temperature, Planck constant, partition functions of the transition state and the reactant, reaction barrier (i.e., the difference of the electronic energies between the transition state and the reactant), and ideal gas constant, respectively.

The reaction class transition state theory (RC-TST) is widely used to calculate the rate coefficients at modest levels using the *ab initio* method for each reaction class.[60,72−76] The basic idea of the RC-TST theory is that the smallest size reaction in a reaction class is regarded as the main reaction, and its accurate rate coefficient k_m can be obtained by a high-level *ab initio* method or an experimental value; the other reactions in the reaction class are regarded as representative reactions and their rate coefficients k_r need to be calculated. In RC-TST, the relationship

https://doi.org/10.1021/acsomega.2c01811
ACS Omega 2022, 7, 20020−20031

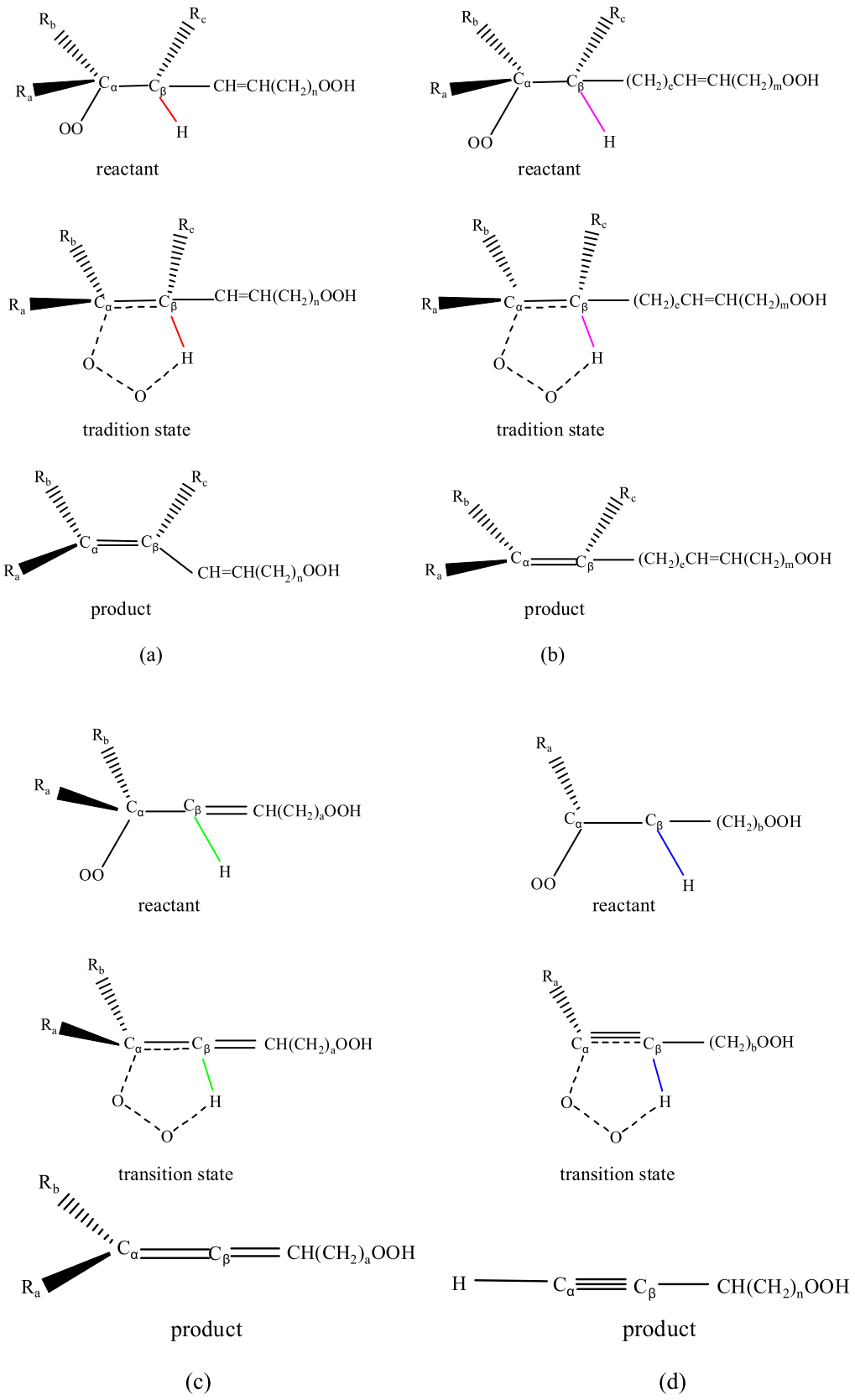

Figure 3. Reaction process for different reaction subclasses: (a) s-allylic subclass; (b) s-alkylic subclass; (c) 1-tv subclass; and (d) 2-tv subclass.

between k_r and k_m can be expressed as $f(T) = \frac{k_r(T)}{k_m(T)} = f_\kappa f_\sigma f_Q f_v f_{HR}$, wherein f_κ, f_σ, f_Q, f_v, and f_{HR} are the transmission, symmetry number, partition function, potential energy, and hindered rotor factors, respectively. These factors are the ratio of the corresponding factors for representative reaction and main reaction. Truong and co-workers observed that the vibrational imaginary frequency of the

https://doi.org/10.1021/acsomega.2c01811
ACS Omega 2022, 7, 20020−20031

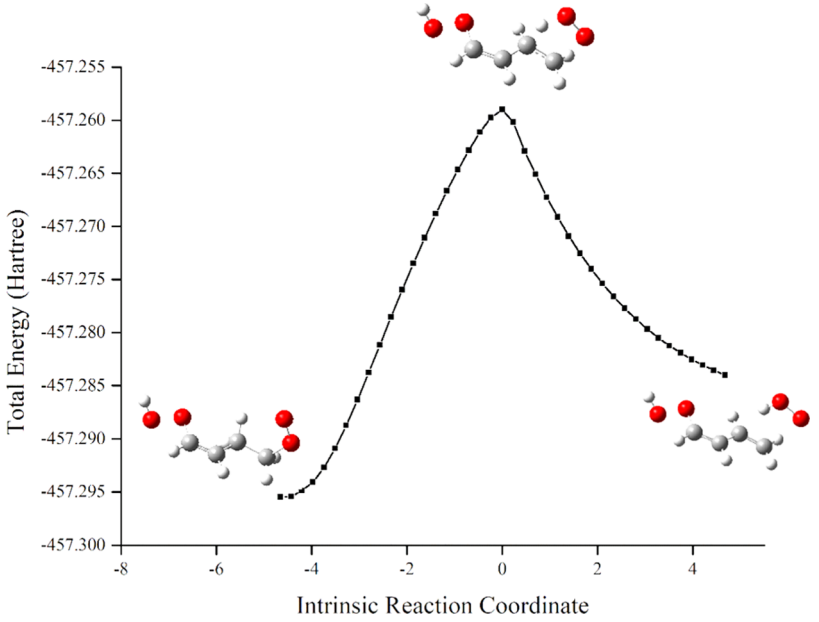

Figure 4. Intrinsic reaction coordinate (IRC) analysis for reaction R1.

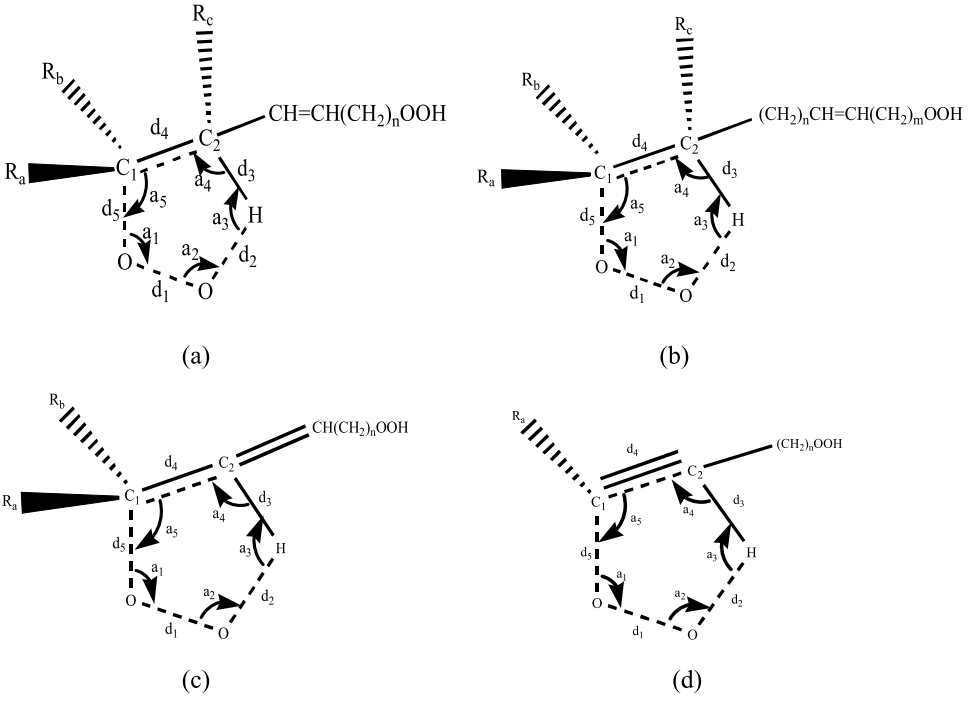

Figure 5. Geometries of the reaction center for the transition states (TS) of different reaction subclasses: (a) s-allylic subclass; (b) s-alkylic subclass; (c) 1-tv subclass; and (d) 2-tv subclass.

transition state is a conserved quantity for different reactions in a reaction class and the partition function can be accurately calculated by a low-level *ab initio* method. More importantly, they found that the accurate potential energy factor can be calculated by a low-level *ab initio* method. Meanwhile, in the work of Wang et al.,[72] they propose an interpretation of the dependence of potential energy factor on the level of the *ab initio* method and extend the isodesmic reaction to the calculation of reaction barriers, reaction enthalpies, and rate coefficients when the main reaction and representative reaction can be combined into a single isodesmic reaction. They point out that the accurate reaction barriers and reaction enthalpies for a representative reaction are the sum of reaction barriers and reaction enthalpies calculated by a low-level *ab initio* method and the correction value, wherein the correction value is the difference of the reaction barrier and reaction enthalpy for the main reaction calculated by the high- and low-level *ab initio* methods, respectively. Similarly, the accurate rate coefficient for a representative reaction is equal to the rate coefficient of the representative reaction calculated by a low-level *ab initio* method time correction factor; the factor is exp $[(-\Delta\Delta V^{\neq})/RT]$, in which $\Delta\Delta V^{\neq}$ is the correction scheme for the reaction barrier from the main reaction.

https://doi.org/10.1021/acsomega.2c01811
ACS Omega 2022, 7, 20020−20031

Table 2. Geometrical Parameters of the Reaction Center for the Transition States of Each Subclass

subclass		d_1/Å	a_1/(°)	d_2/Å	a_2/(°)	d_3/Å	a_3/(°)	d_4/Å	a_4/(°)	d_5/Å	a_5/(°)
s-allylic	[a]avg	1.28	99.60	1.30	97.48	1.34	151.86	1.40	93.16	2.15	97.82
	[b]mad	0.00	1.23	0.01	0.34	0.01	2.50	0.00	0.38	0.06	0.99
	[c]max	0.00	0.72	0.01	0.28	0.01	1.35	0.00	0.27	0.03	0.70
s-alkylic	avg	1.28	97.88	1.29	97.73	1.34	154.26	1.39	93.27	2.22	96.69
	mad	0.00	0.30	0.01	0.12	0.01	0.61	0.00	0.13	0.01	0.21
	max	0.00	0.25	0.01	0.10	0.01	0.59	0.00	0.13	0.01	0.18
1-tv	avg	1.28	97.54	1.24	99.01	1.37	153.51	1.37	96.73	2.27	94.03
	mad	0.03	4.75	0.06	1.08	0.05	3.94	0.01	1.58	0.23	3.61
	max	0.03	4.37	0.06	1.08	0.05	6.06	0.01	1.58	0.22	3.61
2-tv	avg	1.28	97.19	1.25	97.47	1.37	150.51	1.25	96.73	2.19	98.11
	mad	0.00	0.24	0.01	0.30	0.01	0.63	0.00	0.19	0.01	0.19
	max	0.00	0.24	0.01	0.30	0.01	0.63	0.00	0.19	0.01	0.13

[a]The average value of the geometric parameters for the transition states of all reactions in each subclass. [b]The maximum absolute deviation between the different reactions in each subclass. [c]The maximum absolute value of the difference between the main reaction and representative reaction.

3. RESULTS AND DISCUSSION

3.1. Geometries of the Reaction Center for the Transition States. The reaction center for the HO_2 elimination reaction is a five-membered ring in the transition states, and the atoms and bonds involved in the reaction center are shown in Figure 5, wherein "*d*" represents the bond length, "*a*" represents the bond angle, "R" represents the hydrogen or substituent group, C_1 and C_2 are reactive atoms, and "*n*" (n = 0,1,2,3,4,5) and "*m*" (m = 0,1,2,3,4,5) represent the number of methylene radicals attached to the carbon atoms at the left and right ends of the C═C double bond in the reactant molecules, respectively. The optimized geometrical parameters of the reaction centers for the transition states are listed in Table S1 in the Supporting Information. The difference values of the geometrical parameters between the main reaction and representative reaction for each subclass are listed in Table S2 in the Supporting Information. The average values and maximum absolute deviation of the geometrical parameters for all reactions in each subclass of the transition states are listed in Table 2. The maximum absolute value of the difference in geometrical parameters between the main reaction and representative reaction are also listed in Table 2.

From Table 2, it can be seen that the maximum absolute deviations for each subclass of bond lengths and bond angles are 0.06 Å and 2.50°, 0.01 Å and 0.61°, 0.23 Å and 4.75°, and 0.01 Å and 0.63°, respectively. The maximum absolute values of the difference between the main reaction and representative reaction are 0.03 Å and 1.35°, 0.01 Å and 0.59°, 0.22 Å and 6.06°, 0.01 Å and 0.63°. These results show that the geometries

Table 3. Reaction Barriers by the G4 Method and CCSD(T)/cc-pVTZ Method (kcal/mol)[a,b]

	$\Delta V^{\neq}$		
reaction	G4	CCSD(T)/cc-pVTZ	$\Delta V^{\neq\prime}$
R21	45.53	45.17	0.36
R22	45.74	46.36	−0.62

[a]$\Delta V^{\neq\prime}$ the difference of reaction barriers between the G4 and CCSD(T)/cc-pVTZ methods. [b]$\Delta V^{\neq}$ = $\Delta V^{\neq}$(G4)-$\Delta V^{\neq}$ (CCSD(T)/cc-pVTZ).

Table 5. Comparison of the Reaction Barriers (kcal/mol)

	$\Delta V^{\neq}$				
reaction	G4	B3LYP	[a]Δ (DFT)	[b]RC-TST	[c]Δ (RC-TST)
R2	33.55	30.99	2.56	33.50	0.05
R10	34.39	31.87	2.52	35.05	−0.66
R22	45.74	41.70	4.04	45.45	0.29
R32	46.82	46.68	0.14	47.12	−0.30

[a]difference between the G4 and B3LYP methods. [b]the results corrected by RC-TST. [c]difference between G4 and RC-TST.

Table 6. Comparison of the Reaction Enthalpies (kcal/mol)

	$\Delta H^{\neq}$				
reaction	G4	B3LYP	[a]Δ (DFT)	[b]RC-TST	[c]Δ (RC-TST)
R2	15.66	12.13	3.53	15.62	0.04
R10	19.49	17.47	2.02	19.83	−0.34
R22	33.52	30.17	3.35	33.70	−0.18
R32	31.61	33.27	−1.66	31.90	−0.29

[a]difference between the G4 and B3LYP methods. [b]the results corrected by RC-TST. [c]difference between G4 and RC-TST.

Table 4. Reaction Barriers and Enthalpies for Each Subclass of the Main Reaction (kcal/mol)

		[a]$\Delta V^{\neq}$		[b]$\Delta\Delta V^{\neq}$	[c]$\Delta H^{\neq}$		[d]$\Delta\Delta H^{\neq}$
reaction subclass	reaction	G4	B3LYP		G4	B3LYP	
s-allylic	R1	31.46	28.96	2.50	15.99	12.50	3.49
s-alkylic	R9	34.68	31.49	3.19	20.69	18.33	2.36
1-tv	R21	45.53	41.77	3.76	33.45	29.92	3.53
2-tv	R31	47.04	46.60	0.44	31.71	33.08	−1.37

[a]$\Delta V^{\neq}$ reaction barriers. [b]$\Delta\Delta V^{\neq}$ the difference of reaction barriers between the G4 and B3LYP methods. [c]$\Delta H^{\neq}$ reaction enthalpies. [d]$\Delta\Delta H^{\neq}$ the difference of reaction enthalpies between the G4 and B3LYP methods.

https://doi.org/10.1021/acsomega.2c01811
ACS Omega 2022, 7, 20020−20031

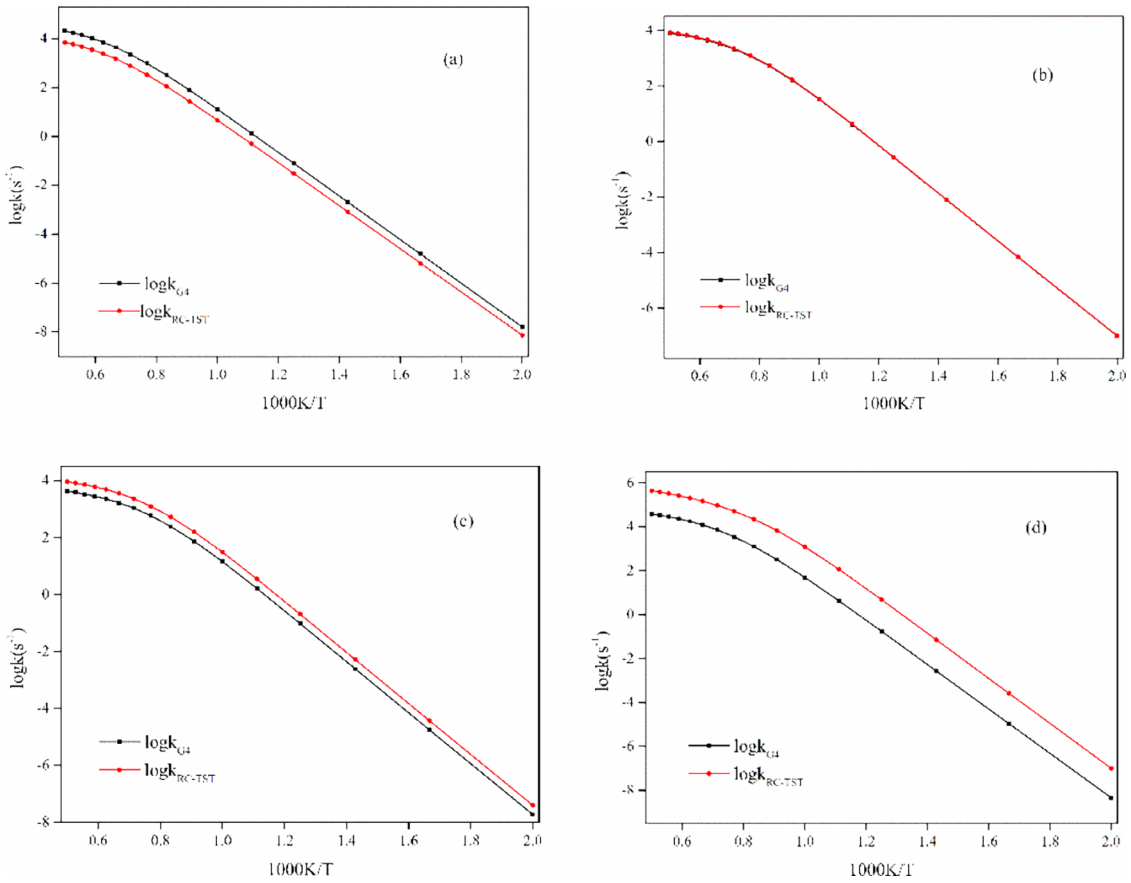

Figure 6. Comparison of the rate coefficients for (a) R22, (b) R23, (c) R24, and (d) R32.

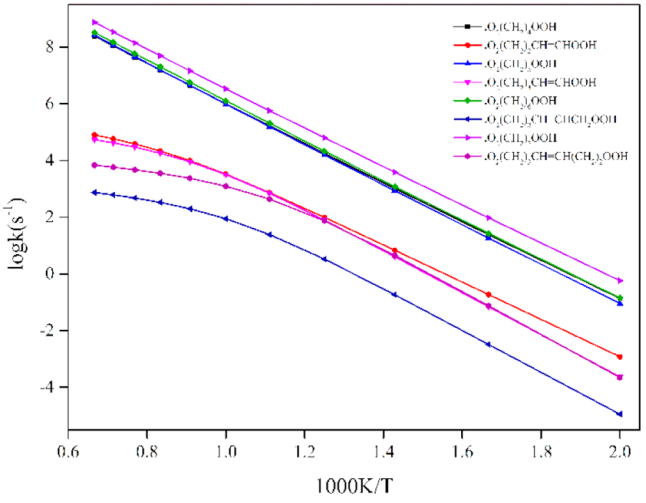

Figure 7. Comparison of the rate coefficients for saturated hydroperoxyalkylperoxy radicals and unsaturated hydroperoxyalkenylperoxy radicals.

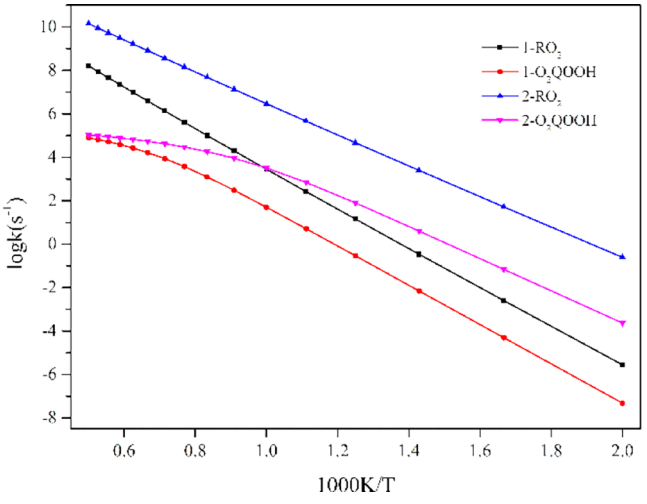

Figure 8. Comparison of the rate coefficients for alkenylperoxy radicals and hydroperoxyalkenylperoxy radicals.

of the reaction centers for the transition states of "s-alkylic" and "2-tv" subclasses are conserved.

3.2. Reaction Barriers and Enthalpies. *3.2.1. Validation of the Reaction Barriers.* In this work, the G4 method is chosen as the high-level *ab initio* method in the correction scheme. To validate the reliability of the reaction barriers, reactions R21 and R22 from Table 1 are selected to compare the reaction barriers by the G4 method and the benchmark CCSD(T)/cc-pVTZ method.[62,63] The results are listed in Table 3.

It can be seen from Table 3 that the reaction barriers for reactions R21 and R22 by the G4 method are close to those of the CCSD(T)/cc-pVTZ method, where the difference of reaction barriers is 0.36 and −0.62 kcal/mol, respectively.

3.2.2. Reaction Barriers and Enthalpies for the Main Reaction of Each Subclass. In this work, reactions R1, R9, R21, and R31 are chosen as the main reactions for each subclass and the other reactions in Table 1 are chosen as representative reactions. The reaction barriers and enthalpies for the main

https://doi.org/10.1021/acsomega.2c01811
ACS Omega 2022, 7, 20020−20031

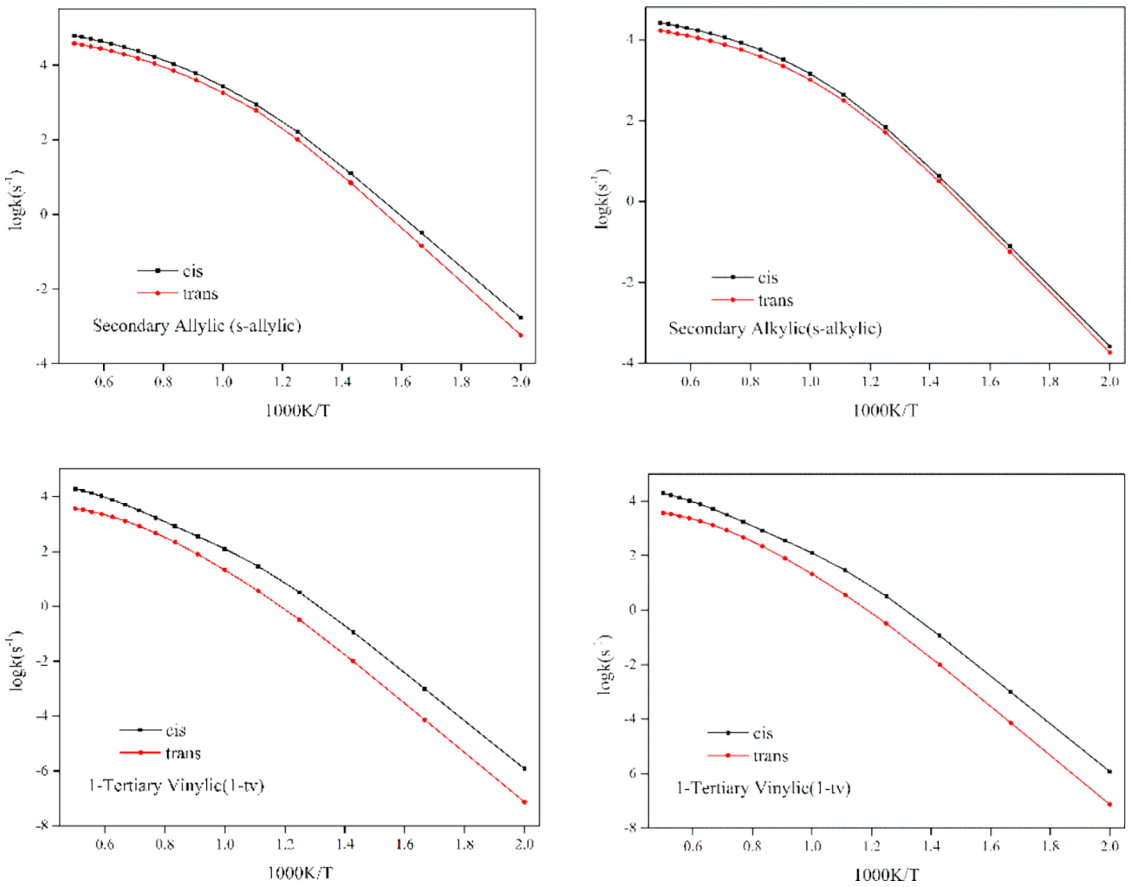

Figure 9. Comparison of the average rate coefficients of *cis*- and trans-hydroperoxyalkenylperoxy radicals.

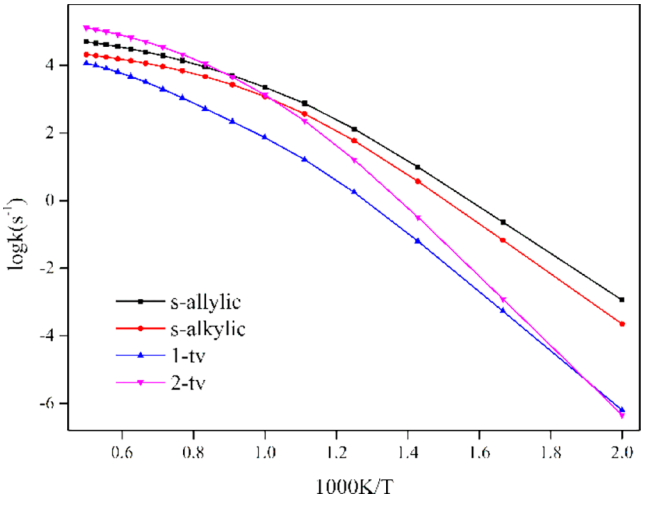

Figure 10. Comparison of the average rate coefficients for different subclasses at 500−2000 K.

reaction at B3LYP and G4 levels, and the difference between the B3LYP and G4 methods of each subclass are listed in Table 4.

It can be seen from Table 4 that the corrected values of the reaction barrier for each subclass are 2.50, 3.19, 3.76, and 0.44 kcal/mol, respectively. The corrected values of the reaction enthalpy for each subclass are 3.49, 2.36, 3.53, and −1.37 kcal/mol, respectively.

3.2.3. Reaction Barriers and Enthalpies for the Representative Reaction. In this part, the reaction barriers and enthalpies for 10 representative reactions are calculated at B3LYP, G4 levels and the corrected value based on RC-TST. The results are listed in Tables 5 and 6. All corrected reaction barriers and enthalpies are listed in Table S3 in the Supporting Information.

It can be seen from Tables 5 and 6 that the absolute values of differences for the reaction barriers and enthalpies by the B3LYP and G4 methods are between 0.14−4.04 and 1.66−3.53 kcal/mol, respectively. However, the differences between the corrected reaction barriers and enthalpies by the RC-TST and G4 methods are reduced to 0.15−0.66 and 0.04−0.34 kcal/mol, respectively.

3.3. High-Pressure-Limit Rate Coefficients and Rate Rules. *3.3.1. High-Pressure-Limit Rate Coefficients.* In this paper, the rate coefficients are compared between the G4 method and RC-TST, which are among the high-level *ab initio* methods and are widely used in the study of the thermochemical properties of different compounds and the study of the kinetics of different reactions.[73] The rate coefficients for reactions R22, R23, R24, and R32 are listed in Table S4 in the Supporting Information. For illustration, Figure 6 shows the difference of the rate coefficients for reactions R22, R23, R24, and R32.

The average ratios of the rate coefficients by the G4 method and RC-TST are 2.76, 0.94, 0.46, and 0.06 between 500−2000 K for reactions R22, R23, R24, and R32, respectively, wherein a large deviation factor of 16.67 of the rate coefficients for "2-tv" subclasses is observed, for which the geometries of the reaction centers for the transition states are conserved.

In order to study the impact of the C═C double bond of the reactant molecules on the rate coefficients, the rate coefficients in the temperature range of 500−1500 K for the saturated hydroperoxyalkylperoxy radicals from reference[77] and for the

https://doi.org/10.1021/acsomega.2c01811
ACS Omega 2022, 7, 20020−20031

Table 7. High-Pressure-Limit Rate Rules for the HO_2 Elimination Reaction

		modified Arrhenius parameters			1000 K
reaction subclass	reaction	A (s^{-1})	n	E (kcal/mol)	[a]f
s-allylic		**4.90×10^{44}**	**−10.71**	**42.50**	
	R1	8.32×10^{44}	−9.67	40.54	1.46
	R2	2.34×10^{44}	−10.39	44.13	0.50
	R3	4.79×10^{44}	−10.78	40.90	0.44
	R4	4.68×10^{44}	−10.66	42.48	0.51
	R5	4.57×10^{44}	−10.92	39.41	0.41
	R6	9.33×10^{44}	−11.23	40.44	0.06
	R7	1.45×10^{45}	−10.96	37.64	2.48
	R8	1.20×10^{45}	−10.90	38.53	2.13
s-alkylic		**4.68×10^{44}**	**−10.77**	**43.42**	
	R9	6.31×10^{44}	−10.51	42.47	2.66
	R10	4.68×10^{44}	−10.53	42.82	1.47
	R11	4.79×10^{44}	−11.10	41.23	0.07
	R12	8.91×10^{44}	−11.07	41.98	0.12
	R13	1.32×10^{45}	−11.01	39.44	1.03
	R14	7.59×10^{44}	−10.97	40.06	0.59
	R15	5.01×10^{44}	−10.91	40.87	0.34
	R16	1.10×10^{45}	−11.15	41.24	0.12
	R17	6.31×10^{44}	−10.94	38.58	1.09
	R18	1.26×10^{45}	−10.97	38.80	1.62
	R19	1.02×10^{45}	−10.94	38.56	1.84
	R20	9.12×10^{44}	−11.00	38.60	1.06
1-tv		**5.13×10^{44}**	**−10.65**	**50.31**	
	R21	7.41×10^{38}	−8.48	53.69	0.69
	R22	4.79×10^{35}	−7.88	51.90	0.06
	R23	5.01×10^{44}	−10.53	53.45	0.47
	R24	4.17×10^{44}	−10.44	54.60	0.42
	R25	4.79×10^{44}	−10.64	50.36	1.68
	R26	7.94×10^{44}	−10.77	52.41	0.42
	R27	1.95×10^{45}	−11.56	49.78	0.02
	R28	2.09×10^{45}	−11.38	50.23	0.06
	R29	1.20×10^{45}	−11.00	45.68	5.70
	R30	2.34×10^{45}	−11.36	47.09	0.46
2-tv		**2.04×10^{45}**	**−10.33**	**53.05**	
	R31	6.17×10^{44}	−9.88	58.62	0.30
	R32	7.76×10^{44}	−9.89	57.01	0.93
	R33	1.78×10^{45}	−10.23	56.09	0.44
	R34	2.09×10^{45}	−10.25	54.70	0.86
	R35	6.92×10^{44}	−10.88	53.13	0.01
	R36	2.14×10^{45}	−10.68	51.63	0.27
	R37	1.66×10^{45}	−10.46	50.30	2.66
	R38	4.07×10^{44}	−10.35	49.02	2.53

[a]$f = k/k_{avg}$ for each subclass; k_{avg} is the average rate coefficient for the reactions in each subclass.

unsaturated hydroperoxyalkenylperoxy radicals in this work are compared. The results are listed in Table S5 in the Supporting Information. Figure 7 shows the difference of the rate coefficients.

It can be seen from Figure 7 that the rate coefficients for the HO_2 elimination reaction of saturated hydroperoxyalkylperoxy radicals are larger than the rate coefficients for unsaturated hydroperoxyalkenylperoxy radicals. The rate coefficients show a similar trend with temperature for the HO_2 elimination reactions of saturated hydroperoxyalkylperoxy radicals and unsaturated hydroperoxyalkenylperoxy radicals, in which the rate coefficients increase with increase in the temperature. However, the difference is that the rate coefficients of the unsaturated hydroperoxyalkenylperoxy radicals increase more slowly than those of saturated hydroperoxyalkylperoxy radicals when the temperature is higher than 1000 K.

In addition, the rate coefficients in the temperature range of 500−2000 K of the HO_2 elimination reaction between the alkenylperoxy radicals from reference[78] and the hydroperoxyalkenylperoxy radicals in this work are also compared. The results are listed in Table S6 in the Supporting Information. Figure 8 plots the comparison of the rate coefficients. In Figure 8, the $CH_2{=}CHCH_2OO^\bullet$ and $CH_2{=}CH(CH_2)_3OO^\bullet$ radicals from reference[78] are represented by 1-RO_2 and 2-RO_2, respectively. The $HOOCH{=}CHCH_2OO^\bullet$ and $HOOCH{=}CH(CH_2)_3OO^\bullet$ radicals in this work are represented by 1-O_2QOOH and 2-O_2QOOH, respectively.

It can be seen from Figure 8 that the rate coefficients for the HO_2 elimination reaction of alkenylperoxy radicals are larger than the rate coefficients of hydroperoxyalkenylperoxy radicals. However, the impact of the molecular size on the rate coefficients of hydroperoxyalkenylperoxy radicals is different from that for the rate coefficients of alkenylperoxy radicals. When the temperature is higher than 1500 K, the rate coefficients tend to change gently with the molecular size. Therefore, the study of the HO_2 elimination reaction for hydroperoxyalkenylperoxy radicals will be of great significance for understanding the impact of molecular size on the reaction reactivity between one-step and two-step oxygenation in the low-temperature reaction mechanism of alkenyl radicals.

In this work, the impact of configurations of the reactant molecules on the rate coefficients is also considered; the comparison of the average rate coefficients for the *cis*- and trans-configuration reactant molecules of each subclass at 500, 1000, 1500, and 2000 K is shown in Table S7 in the Supporting Information. For illustration, Figure 9 shows the impact of configurations of the reactants on the rate coefficients.

It can be seen from Figure 9 that the average rate coefficients of *cis*-hydroperoxyalkenylperoxy radicals are larger than the average rate coefficients of trans-hydroperoxyalkenylperoxy radicals for "s-allylic", "s-alkylic", and "1-tv" subclasses. However, the average rate coefficients of trans-hydroperoxy-alkyl-peroxy radicals are larger than the average rate coefficients of *cis*-hydroperoxy-alkyl-peroxy radicals for the "2-tv" subclass.

In addition, the impact of the types of C−H bonds on the rate coefficients is shown in Figure 10. It can be seen from Figure 10 that when the temperature is lower than 1000 K, the high-pressure-limit rate coefficients exhibit the following tendency: "s-allylic"> "s-alkylic"> "2-tv"> "1-tv"; when the temperature range is 1000−1200 K, the rate coefficients exhibit the following tendency: "s-allylic">"2-tv"> "s-alkylic"> "1-tv"; when the temperature is larger than 1200 K, the high-pressure-limit rate coefficients exhibit the following tendency: "2-tv"> "s-allylic> "s-alkylic"> "1-tv".

3.3.2. High-Pressure-Limit Rate Rules. The reaction rate rules in the high-pressure limit for each subclass are derived by taking the average of the rate coefficients from a representative set of reactions with different numbers of carbon atoms. The fitted (A, n, E) parameters in the high-pressure limit from 500 to 2000 K for all reactions are listed in Table 7. Meanwhile, the ratio f at 1000 K is used to evaluate the uncertainty of the rate rules.

It can be seen from Table 7 that the ranges of the ratio for each subclass are within 0.06−2.48, 0.07−2.66, 0.02−5.70, and 0.01−2.66 for the "s-allylic" subclass, "s-alkylic" subclass, "1-tv"

https://doi.org/10.1021/acsomega.2c01811
ACS Omega 2022, 7, 20020−20031

subclass, and "2-tv" subclass, respectively. This indicates that the rate rules obtained by taking the average of the rate coefficients from representative reactions have a large deviation.

4. CONCLUSIONS

In this work, we report the reaction barriers, enthalpies, and rate coefficients for the HO_2 elimination reaction of hydroperoxyalkenylperoxy radicals based on RC-TST. The high-pressure-limit rate coefficients and rate rules at 500−2000 K are calculated for the reaction class. The deviations of the reaction barriers and enthalpies for reactions R2, R10, R22, and R32 between B3LYP/6-31+G(d,p) and G4 methods are more than 1 kcal/mol, while the deviations are reduced to less than 1 kcal/mol after correction by the RC-TST method. Meanwhile, the deviation factor of rate coefficients for reaction R32 of "2-tv" subclasses is 16.67, which indicates that the geometries of the reaction centers for the transition states are conserved. In addition, the ranges of the uncertainty factor for the rate rules are within 0.06−2.48, 0.07−2.66, 0.02−5.70, and 0.01−2.66 for "s-allylic", "s-alkylic", "1-tv", and "2-tv" subclasses, respectively, indicating that there is a large uncertainty in the rate rules by taking the average of rate coefficients for the representative reactions in the reaction subclass.

Through the comparison of rate coefficients for saturated hydroperoxyalkylperoxy radicals and unsaturated hydroperoxyalkenylperoxy radicals, the results show that the C═C double bond on the rate coefficients of unsaturated hydroperoxyalkenylperoxy radicals increases more slowly than that of saturated hydroperoxyalkylperoxy radicals when the temperature is higher than 1000 K. The impact of the molecular size on the rate coefficients for alkenylperoxy radicals and hydroperoxyalkenylperoxy radicals is that the rate coefficients tend to change gently with the molecular size when the temperature is higher than 1500 K. Therefore, it is necessary to study the HO_2 elimination reaction for the hydroperoxyalkenylperoxy radicals. In addition, the impact of configurations of the reactants on the rate coefficients exhibits the following tendency: k(cis)> k(trans) for "s-allylic", "s-alkylic", and "1-tv" subclasses, while k(trans)> k(cis) for the "2-tv" subclass. At the same time, the rate coefficients of the different types of C−H in the different temperature ranges show the following trend: "s-allylic"> "s-alkylic"> "2-tv"> "1-tv" (T<1000 K), "s-allylic"> "2-tv"> "s-alkylic"> "1-tv" (1000 K<T<1200 K), and "2-tv"> "s-allylic"> "s-alkylic"> "1-tv" (T>1200 K).

ASSOCIATED CONTENT

Supporting Information

The Supporting Information is available free of charge at https://pubs.acs.org/doi/10.1021/acsomega.2c01811.

Optimized geometrical parameters of the reaction centers for transition states, the difference of the geometrical parameters between the main reaction and representative reactions, the reaction barriers and enthalpies for all reactions, the comparison of the rate coefficients by G4 method and the RC-TST, the comparison of the rate coefficients for saturated hydroperoxyalkylperoxy and unsaturated hydroperoxyalkenylperoxy radicals, the comparison of the rate coefficients for alkenylperoxy radicals and hydroperoxyalkenylperoxy radicals, the comparison of the average rate coefficients for cis- with trans-reaction molecules, the cartesian coordinates for all transition states and the intrinsic reaction coordinate (IRC) analysis for reaction R1 to R38 (PDF)

AUTHOR INFORMATION

Corresponding Author

XiaoHui Sun − *School of Energy Industry, Shanxi College of Technology, Shuozhou 036000, P. R. China; College of Chemistry, Sichuan University, Chengdu 610064, P. R. China;* orcid.org/0000-0002-5036-9047; Email: xiaohuisun526@foxmail.com

Authors

ZhenYu Pei − *School of Energy Industry, Shanxi College of Technology, Shuozhou 036000, P. R. China*

ZeRong Li − *College of Chemistry, Sichuan University, Chengdu 610064, P. R. China;* orcid.org/0000-0003-1712-7158

Complete contact information is available at: https://pubs.acs.org/10.1021/acsomega.2c01811

Notes

The authors declare no competing financial interest.

ACKNOWLEDGMENTS

This work is supported by the Scientific and Technologial Innovation Programs of Higher Education Institutions in Shanxi (STIP 2021L604 and 2021L605).

REFERENCES

(1) Zhou, C. W.; Farooq, A.; Yang, L. J.; Mebel, A. M. Combustion chemistry of alkenes and alkadienes. *Pro. Energy Combust. Sci.* **2022**, *90*, No. 100983.

(2) Zádor, J.; Taatjes, C. A.; Fernades, R. X. Kinetic of elementary reactions in low-temperature autoignition chemistry. *Pro. Energy. Combust Sci.* **2011**, *37*, 371−421.

(3) Yao, X. X.; Pang, W. Q.; Li, T.; Shentu, J. T.; Li, Z. R.; Z Q; Li, X. Y. High-pressure-limit and pressure-dependent rate rules for unimolecular reactions related to hydroperoxy alkyl radicals in normal-alkyl cyclohexane combustion. 2. cyclization reaction class. *J. Phys. Chem. A* **2021**, *125*, 8959−8977.

(4) Mehl, M.; Vanhove, G.; Pitz, W. J.; Ranzi, E. Oxidation and combustion of the n-hexene isomers: a wide range kinetic modeling study. *Combust. Flame* **2008**, *155*, 756−772.

(5) Mehl, M.; Pitz, W. J.; Westbrook, C. K.; Curran, H. J. Kinetic modeling of gasoline under engine conditions. *Proc. Combust. Inst.* **2011**, *33*, 193−200.

(6) Pasternak, M.; Mauss, F.; Bensler, H. Diesel engine cycle simulation with a reduced set of modeling parameters based on detailed kinetics, *SAE Technical Paper*, **2009**, 2009-01-0676. DOI: 10.4271/2009-01-0676.

(7) Liu, Z.; Chen, R. A zero-dimensional combustion model with reduced kinetics for SI engine knock simulation. *Combust. Sci. Technol.* **2009**, *181*, 828−852.

(8) Naik, C. V.; Pitz, W. J.; Sjöberg, M.; Dec, J. E.; Orme, J.; Curran, H. J.; Simmie, J. M.; Westbrook, C. K. Detailed chemical kinetic modeling of surrogate fuels for gasoline and application to an HCCI Engine. *SAE Trans.* **2005**, *114*, 1381−1387.

(9) Minetti, R.; Roubaud, A.; Therssen, E.; Ribaucour, M.; Sochet, L. R. The chemistry of pre-ignition of n-pentane and 1-pentene. *Combust. Flame* **1999**, *118*, 213−220.

(10) Ribaucour, M.; Minetti, R.; Sochet, L. R. Autoignition of n-pentane and 1-pentene: experimental data and kinetic modeling. *Symp. Int. Combust.* **1998**, *27*, 345−351.

(11) Touchard, S.; Fournet, R.; Glaude, P. A.; Warth, V.; Battin-Leclerc, F.; Vanhove, G.; Ribaucour, M.; Minetti, R. Modeling of the oxidation of large alkenes at low temperature. *Proc. Combust. Inst.* **2005**, *30*, 1073−1081.

(12) Violi, A.; Yan, S.; Eddings, E. G.; Sarofim, A. F.; Granata, S.; Faravelli, T.; Ranzi, E. Experimental formulation and kinetic model for JP-8 surrogate mixtures. *Combust. Sci. Technol.* **2002**, *174*, 399−417.
(13) Peters, N. *Turbulent Combustion (Cambridge Monographs on Mechanics Cambridge)*; University Press: Cambridge, 2000.
(14) Pitsch, H. Large eddy simulations of turbulent combustion. *Annu. Rev. Fluid Mech.* **2006**, *38*, 453−482.
(15) Truong, T. N.; Duncan, W. T.; Tirtowidjojo, M. A reaction class approach for modeling gas phase reaction rates. *Phys. Chem. Chem. Phys.* **1999**, *1*, 1061−1065.
(16) Sun, X. H.; Zong, W. G.; Wang, J.; Li, Z. R.; Li, X. Y. Pressure-dependent rate rules for cycloaddition, intramolecular H-shift, and concerted elimination reactions of alkenyl peroxy radicals at low temperature. *Phys. Chem. Chem. Phys.* **2019**, *21*, 10693−10705.
(17) Magoon, G. R.; Green, W. H. Design and implementation of a next-generation software interface for on-the-fly quantum and force field calculations in automated reaction mechanism generation. *Comput. Chem. Eng.* **2013**, *52*, 35−45.
(18) Green, W. H.; West, R. H. Release 2019-12: RMG-Reaction Mechanism Generator; open-source software. 2019, http://rmg.mit.edu.
(19) Van Geem, K. M.; Reyniers, M. F.; Marin, G. B.; Song, J.; Green, W. H.; Matheu, D. M. Automatic reaction network generation using RMG for steam cracking of n-hexane. *AIChE J.* **2006**, *52*, 718−730.
(20) Blurock, E. S. Reaction: system for modeling chemical reactions. *J. Chem. Inf. Comput. Sci.* **1995**, *35*, 607−616.
(21) Blurock, E. S. Detailed mechanism generation. 1. Generalized reactive properties as reaction class substructures. *J. Chem. Inf. Comput. Sci.* **2004**, *44*, 1336−1347.
(22) Moréac, G.; Blurock, E. S.; Mauss, F. Automatic generation of a detailed mechanism for the oxidation of n-decane. *Combust. Sci. Technol.* **2006**, *178*, 2025−2038.
(23) Battin-Leclerc, F.; Glaude, P. A.; Warth, V.; Fournet, R.; Scacchi, G.; Côme, G. M. Computer tools for modelling the chemical phenomena related to combustion. *Chem. Eng. Sci.* **2000**, *55*, 2883−2893.
(24) Glaude, P. A.; Warth, V.; Fournet, R.; Battin-Leclerc, F.; Scacchi, G.; Côme, G. M. Modeling of the oxidation of n-octane and n-decane using an automatic generation of mechanisms. *Int. J. Chem. Kinet.* **1998**, *30*, 949−959.
(25) Miyoshi, A. KUCRS-What is KUCRS? Miyoshi, A., Ed., 2011. http://www.frad.t.u-tokyo.ac.jp/~miyoshi/KUCRS/ (accessed December 26, 2006).
(26) Ranzi, E.; Dente, M.; Goldaniga, A.; Bozzano, G.; Faravelli, T. Lumping procedures in detailed kinetic modeling of gasification, pyrolysis, partial oxidation and combustion of hydrocarbon mixtures. *Prog. Energy Combust. Sci.* **2001**, *27*, 99−139.
(27) Ranzi, E.; Sogaro, A.; Gaffuri, P.; Pennati, G.; Westbrook, C. K.; Pitz, W. J. A new comprehensive reaction mechanism for combustion of hydrocarbon fuels. *Combust. Flame* **1994**, *99*, 201−211.
(28) Sun, X. H.; Zong, W. G.; Li, Z. R.; Li, X. Y. Pressure-dependent rate rules for the intramolecular H-shift reactions of hydroperoxy-alkenyl-peroxy radicals in low temperature. *Energy Fuels* **2019**, *33*, 5597−5609.
(29) Wang, H.; You, X. Q.; Joshi, A. V.; Davis, S. G.; Laskin, A.; Egolfopoulos, F.; Law, C. K. Release 2007-05: USC Mech Version II. High-Temperature Combustion Reaction Model of H2/CO/C1-C4 Compounds, 2007. http://ignis.usc.edu/USC_Mech_II.htm.
(30) Smith, G. P.; Golden, D. M.; Frenklach, M.; Moriarty, N. W.; Eiteneer, B.; Goldenberg, M.; Bowman, C. T.; Hanson, R. K.; Song, S.; Gardiner, W. C., Jr.; Lissianski, V. V.; Qin, Z. Release 1999-01: GRI-Mech 3.0; 1999, http://www.me.berkeley.edu/gri_mech/ (accessed Oct 10, 2012).
(31) Center for Energy Research. *Chemical Kinetic Mechanism for Combustion Application*; University of California: San Diego, CA, USA, 2012.
(32) Manente, V.; Johansson, B.; Cannella, W. Gasoline partially premixed combustion, the future of internal combustion engines. *Int. J. Engine Res.* **2011**, *12*, 194−208.
(33) Reitz, R. D.; Duraisamy, G. Review of high efficiency and clean reactivity controlled compression ignition (RCCI) combustion in internal combustion engines. *Prog. Energy Combust. Sci.* **2015**, *46*, 12−71.
(34) Yao, M.; Zheng, Z.; Liu, H. Progress and recent trends in homogeneous charge compression ignition (HCCI) engines. *Prog. Energy Combust. Sci.* **2009**, *35*, 398−437.
(35) Wang, Q. D. Theoretical studies of unimolecular thermal decomposition reactions of n-hexane and n-hexene isomers. *Comput. Theor. Chem.* **2017**, *1115*, 45−55.
(36) Wang, Z.; Herbinet, O.; Hansen, N.; Battin-Leclerc, F. Exploring hydroperoxides in combustion: History, recent advances and perspectives. *Prog. Energy Combust. Sci.* **2019**, *73*, 132−181.
(37) Mehl, M.; Faravelli, T.; Ranzi, E.; Ciajolo, A.; Tregrossi, A. In *A Wide Range Kinetic Modeling Study of Alkene Oxidation*, Proceedings of the 29th Combustion Meeting. Italian Section of the Combustion Institute, 2006.
(38) Metcalfe, W. K.; Burke, S. M.; Ahmed, S. S.; Curran, H. J. A hierarchical and comparative kinetic modeling study of C1-C2 hydrocarbon and oxygenated fuels. *Int. J. Chem. Kinet.* **2013**, *45*, 638−675.
(39) Xu, C.; Konnov, A. A. Validation and analysis of detailed kinetic models for ethylene combustion. *Energy* **2012**, *43*, 19−29.
(40) Konnov, A. A. Implementation of the NCN pathway of prompt-NO formation in the detailed reaction mechanism. *Combust. Flame* **2009**, *156*, 2093−2105.
(41) Center for Energy research. *Chemical Kinetic Mechanism for Combustion Application*; University of California: San Diego, http://combustion.ucsd.edu (accessed accessed Oct 1, 2019).
(42) Wang, H.; You, X. Q.; Joshi, A. V.; Davis, S. G.; Laskin, A.; Egolfopoulos, F.; Law, C. K. Release 2007-05: USC mech version II. High-temperature combustion reaction model of H2/CO/C1-C4 compounds. 2007. http://ignis.usc.edu/USC_Mech_II.htm (accessed accessed Oct 1, 2019).
(43) Kikui, S.; Nakamura, H.; Tezuka, T.; Hasegawa, S.; Maruta, K. Study on combustion and ignition characteristics of ethylene, propylene, 1-butene and 1-pentene in a micro flow reactor with a controlled temperature profile. *Combust. Flame* **2016**, *163*, 209−219.
(44) Cong, T. L.; Bedjanian, E.; Dagaut, P. Oxidation of ethylene and propene in the presence of CO_2 and H_2O: experimental and detailed kinetic modeling study. *Combust. Sci. Technol.* **2010**, *182*, 333−349.
(45) Dagaut, P.; Cathonnet, M.; Boettner, J. C. Experimental study and kinetic modeling of propene oxidation in a jet stirred flow reactor. *J. Phys. Chem. A* **1988**, *92*, 661−671.
(46) Davis, S. G.; Law, C. K.; Wang, H. Propene pyrolysis and oxidation kinetics in a flow reactor and laminar flames. *Combust. Flame.* **1999**, *119*, 375−399.
(47) Westbrook, C. K.; Pitz, W. J. A comprehensive chemical kinetic reaction mechanism for oxidation and pyrolysis of propane and propene. *Combust. Sci. Technol.* **1984**, *37*, 117−152.
(48) Goldaniga, A.; Faravelli, T.; Ranzi, E. The kinetic modeling of soot precursors in a butadiene flame. *Combust. Flame* **2000**, *122*, 350−358.
(49) Zhou, C. W.; Li, Y.; Burke, U.; Banyon, C.; Somers, K. P.; Ding, S.; Saadat, K.; Joshua, W. H.; Travis, S.; Olivier, M.; Eric, L. P.; Mohammed, A.; Aamir, F.; Pan, Y.; Zhang, Y.; Huang, Z.; Joseph, L.; Zachary, L.; Subith, S. V.; Henry, J. C. An experimental and chemical kinetic modeling study of 1,3-butadiene combustion: ignition delay time and laminar flame speed measurements. *Combust. Flame* **2018**, *197*, 423−438.
(50) de Goey, L. P. H.; van Maaren, A.; Quax, R. M. Stabilization of adiabatic premixed laminar flames on a flat flame burner. *Combust. Sci. Technol.* **1993**, *92*, 201−207.
(51) Hellier, P.; Ladommatos, N.; Allan, R.; Rogerson, J. Combustion and emissions characteristics of toluene/n-heptane and 1-octene/n-octane binary mixtures in a direct injection compression ignition engine. *Combust. Flame* **2013**, *160*, 2141−2158.

https://doi.org/10.1021/acsomega.2c01811
ACS Omega 2022, 7, 20020−20031

(52) Hellier, P.; Ladommatos, N.; Allan, R.; Filip, S.; Rogerson, J. The importance of double bond position and cis-trans isomerisation in diesel combustion and emissions. *Fuel* **2013**, *105*, 477−489.
(53) Meng, X. Z.; Herbinet, O.; Wang, T. Y.; Battin-Leclerc, F. Experimental and modeling study of 1-octene jet-stirred reactor oxidation. *Fuel* **2017**, *207*, 763−775.
(54) Shang-Jun, L.; Tan, N. X.; Yao, Q.; Li, Z. R.; Li, X. Y. Calculation of Rate Constants for Intramolecular Hydrogen Migration Reactions of Alkylperoxy Radicals. *Acta Phys.-Chim. Sin.* **2015**, *31*, 859−865.
(55) Yao, Q.; Sun, X. H.; Li, Z. R.; Chen, F. F.; Li, X. Y. Pressure-dependent rate rules for intramolecular H-migration reactions of hydroperoxyalkylperoxy radicals in low temperature. *J. Phys. Chem. A* **2017**, *121*, 3001−3018.
(56) Villano, S. M.; Huynh, L. K.; Caestensen, H. H.; Dean, A. M. High-pressure rate rules for alkyl + O_2 reactions. 1. the dissociation, concerted elimination, and isomerization channels of the alkyl peroxy radical. *J. Phys. Chem. A* **2011**, *115*, 13425−13442.
(57) Huynh, L. K.; Carstensen, H. H.; Dean, A. M. Detailed modeling of low-temperature propane oxidation: 1. the role of the propyl +O_2 reaction. *J. Phys. Chem. A* **2010**, *114*, 6594−6607.
(58) Wang, K.; Villano, S. M.; Dean, A. M. Reactivity-structure-based rate estimation rules for alkyl radical H atom shift and alkenyl radical cycloaddition reactions. *J. Phys. Chem. A* **2015**, *119*, 7205−7221.
(59) Villano, S. M.; Huynh, L. K.; Caestensen, H. H.; Dean, A. M. High-pressure rate rules for alkyl + O_2 Reactions. 2. the isomerization, cyclic ether formation, and β-scission reactions of hydroperoxy alkyl radicals. *J. Phys. Chem. A* **2012**, *116*, 5068−5089.
(60) Li, Y. Q.; Yao, X. X.; Sun, X. H.; Li, Z. R.; Wang, J. B.; Li, X. Y. Automatic construction of transition states and on-the-fly accurate kinetic calculations for reaction classes in automated mechanism generators. *Comput. Theor. Chem.* **2020**, *1184*, No. 112852.
(61) Frisch, M. J.; Trucks, G. W.; Schlegel, H. B.; Scuseria, G. E.; Robb, M. A.; Cheeseman, J. R.; Scalmani, G.; Barone, V.; Mennucci, B.; Petersson, G. A.; Nakatsuji, H.; Li, X.; Caricato, M.; Marenich, A.; Bloino, J.; Janesko, B. G.; Gomperts, R.; Mennucci, B.; Hratchian, H. P.; Ortiz, J. V.; Izmaylov, A. F.; Sonnenberg, J. L.; Williams-Young, D.; Ding, F.; Lipparini, F.; Egidi, F.; Goings, J.; Peng, B.; Petrone, A.; Henderson, T.; Ranasinghe, D.; Zakrzewski, V. G.; Gao, J.; Rega, N.; Zheng, G.; Liang, W.; Hada, M.; Ehara, M.; Toyota, K.; Fukuda, R.; Hasegawa, J.; Ishida, M.; Nakajima, T.; Honda, Y.; Kitao, O.; Nakai, H.; Vreven, T.; Throssell, K.; Montgomery, J. A., Jr.; Peralta, J. E.; Ogliaro, F.; Bearpark, M.; Heyd, J. J.; Brothers, E.; Kudin, K. N.; Staroverov, V. N.; Keith, T.; Kobayashi, R.; Normand, J.; Raghavachari, K.; Rendell, A.; Burant, J. C.; Iyengar, S. S.; Tomasi, J.; Cossi, M.; Millam, J. M.; Klene, M.; Adamo, C.; Cammi, R.; Ochterski, J. W.; Martin, R. L.; Morokuma, K.; Farkas, O.; Foresman, J. B.; Fox, D. J. *Release 2016: Gaussian 09*, Revision A. I.; Gaussian, Inc.: Wallingford, CT, USA, https://gaussian.com, 2016.
(62) Goldsmith, C. F.; Magoon, G. R.; Green, W. H. Database of small molecule thermochemistry for combustion. *J. Phys. Chem. A* **2012**, *116*, 9033−9057.
(63) Pollack, L.; Windus, T. L.; de Jong, W. A.; Dixon, D. A. Thermodynamic properties of the C5, C6, and C8 n-alkanes from ab initio electronic structure theory. *J. Phys. Chem. A* **2005**, *109*, 6934−6938.
(64) Klippenstein, S. J.; Pande, V. S.; Truhlar, D. G. Chemical kinetics and mechanisms of complex system: A perspective on recent theoretical advances. *J. Am. Chem. Soc.* **2014**, *136*, 528−546.
(65) Pitzer, K. S.; Gwinn, W. D. Energy levels and thermodynamic functions for molecules with internal rotation: I. Rigid frame with attached tops. *J. Chem. Phys.* **1942**, *10*, 428−440.
(66) Mammen, M.; Shakhnovich, E. I.; Whitesides, G. M. Using a convenient, quantitative model for torsional entropy to establish qualitative trends for molecular processes that restrict conformational freedom. *J. Org. Chem.* **1998**, *63*, 3168−3175.
(67) Mokrushin, V.; Tsang, W. *Release 2009: Chemrate, v.1.5.8*; National Institute of Standards and Technology: Gaithersburg, MD, 2009. https://kinetics.nist.gov/ChemRate/.
(68) Eckart, C. The Penetration of a Potential Barrier by Electrons. *Phys. Rev.* **1930**, *35*, 1303−1309.
(69) Johnston, H. S.; Heicklen, J. Tunnelling Corrections for Unsymmetrical Eckart Potential Energy Barriers. *J. Phys. Chem. B* **1962**, *66*, 532−533.
(70) Zhang, F.; Dibble, T. S. Impact of Tunneling on Hydrogen-Migration of the N-Propylperoxy Radical. *Phys. Chem. Chem. Phys.* **2011**, *13*, 17969−17977.
(71) Glasstone, S.; Laidler, K. J.; Eyring, H. *The Theory of Rate Processes*; McGraw-Hill: New York, 1941.
(72) Wang, B. Y.; Li, Z. R.; Tan, N. X.; Yao, Q.; Li, X. Y. Interpretation and application of reaction class transition state theory for accurate calculation of thermokinetic parameters using isodesmic reaction method. *J. Phys. Chem. A* **2013**, *117*, 3279−3291.
(73) Curtiss, L. A.; Redfern, P. C.; Raghavachari, K. Assessment of Gaussian-4 theory for energy barriers. *Chem. Phys. Lett.* **2010**, *499*, 168−172.
(74) Wang, Q. D.; Wang, X. J.; Kang, G. J. An application of the reaction class transition state theory to the kinetics of hydrogen abstraction reactions of hydrogen with methyl esters at the methoxy group. *Comput. Thoer. Chem.* **2014**, *1027*, 103−111.
(75) Ratkiewicz, A.; Huynh, L. K.; Troung, T. N. Performance of first-principles-based reaction class transition state theory. *J. Phys. Chem. B* **2016**, *120*, 1871−1884.
(76) Truong, T. N. Reaction class transition state theory: hydrogen abstraction reactions by hydrogen atoms as test cases. *J. Chem. Phys.* **2000**, *113*, 4957−4964.
(77) Sun, X. H.; Yao, Q.; Li, Z. R.; Wang, J. B.; Li, X. Y. Calculation of the rate constants for concerted elimination reaction class of hydroperoxyl-alkyl-peroxyl radicals. *Theor. Chem. Acc.* **2017**, *136*, No. 64.
(78) Zhang, F.; Dibble, T. S. Effects of olefin group and its position on the kinetics for intramolecular H-shift and HO2 elimination of alkenyl peroxy radicals. *J. Phys. Chem. A* **2011**, *115*, 655−663.

https://doi.org/10.1021/acsomega.2c01811
ACS Omega 2022, 7, 20020−20031